Conformational plasticity of phospholipid headgroups in simulations and experiments

Amélie Bacle,[1] Pavel Buslaev,[2, 3] Rebeca García Fandiño,[4, 5] Fernando Favela-Rosales,[6] Tiago M. Ferreira,[7] Patrick F.J. Fuchs,[8, 9] Ivan Gushchin,[3] Matti Javanainen,[10] Anne M. Kiirikki,[11] Jesper J. Madsen,[12, 13] Josef Melcr,[14] Paula Milán Rodríguez,[8] Markus S. Miettinen,[15] O. H. Samuli Ollila,[11, *] Chris G. Papadopoulos,[16] Antonio Peón,[5] Thomas J. Piggot,[17] Ángel Piñeiro,[18] and Salla I. Virtanen[11]

[1]*Laboratoire Coopératif "Lipotoxicity and Channelopathies - ConicMeds",*
Université de Poitiers, 1 rue Georges Bonnet, 86000 Poitiers, France
[2]*Nanoscience Center and Department of Chemistry, University of Jyvskyl, P.O. Box 35, 40014 Jyvskyl, Finland*
[3]*Research Center for Molecular Mechanisms of Aging and Age-related Diseases,*
Moscow Institute of Physics and Technology, 141701 Dolgoprudny, Russia
[4]*Center for Research in Biological Chemistry and Molecular Materials (CiQUS),*
Universidade de Santiago de Compostela, E-15782 Santiago de Compostela, Spain
[5]*CIQUP, Centro de Investigao em Química, Departamento de Química e Bioquímica,*
Faculdade de Ciências, Universidade do Porto, Porto, Portugal
[6]*Departamento de Ciencias Básicas, Tecnológico Nacional de México - ITS Zacatecas Occidente, México*
[7]*NMR group - Institute for Physics, Martin Luther University Halle-Wittenberg, 06120 Halle (Saale), Germany*
[8]*Sorbonne Université, Ecole Normale Supérieure, PSL University,*
CNRS, Laboratoire des Biomolécules (LBM), 75005 Paris, France
[9]*Université de Paris, UFR Sciences du Vivant, 75013, Paris, France*
[10]*Institute of Organic Chemistry and Biochemistry of the Czech Academy of Sciences,*
Flemingovo nám. 542/2, CZ-16610 Prague 6, Czech Republic
[11]*Institute of Biotechnology, University of Helsinki*
[12]*Department of Chemistry, The University of Chicago, Chicago, Illinois, United States of America*
[13]*Global and Planetary Health, College of Public Health,*
University of South Florida, Tampa, Florida, United States of America
[14]*Groningen Biomolecular Sciences and Biotechnology Institute and The Zernike Institute for Advanced Materials,*
University of Groningen, 9747 AG Groningen, The Netherlands
[15]*Department of Theory and Bio-Systems, Max Planck Institute of Colloids and Interfaces, 14424 Potsdam, Germany*
[16]*Université Paris-Saclay, CEA, CNRS, Institute for Integrative Biology of the Cell (I2BC), 91198 Gif-sur-Yvette, France*
[17]*Chemistry, University of Southampton, Highfield, Southampton SO17 1BJ, United Kingdom*
[18]*Departamento de Física Aplicada, Facultade de Física,*
Universidade de Santiago de Compostela, E-15782 Santiago de Compostela, Spain
(Dated: May 5, 2021)

The chemistry of lipid headgroups, the water-facing interface of cellular membranes, regulates cell functions via lipid–protein interactions. In the physiologically relevant liquid state, lipid molecules are not fixed to a single structure but sample an ensemble of conformations with Boltzmann-weighted probabilities. However, the distributions of conformations in such ensembles and their lipid-type dependence have not yet been experimentally determined: It is not clear if lipid molecules exchange between a few rigid structures, or fluctuate freely across a practically continuous spectrum of conformations. Here, we combine solid-state NMR experiments and molecular dynamics simulations from the NMRlipids Project to resolve the conformational ensembles of headgroups of four key lipid types in various biologically relevant conditions. We find all lipid headgroup types to sample a wide range of conformations in both neutral and charged cellular membranes. Differences in the headgroup chemistry do manifest in probability distributions of conformations, but all four lipid types can access almost the whole conformation range. Together with the analysis of 894 protein-bound lipid structures from the Protein Data Bank (PDB), this suggests that lipids can bind to proteins in a wide range of conformations, which are not limited by the headgroup chemistry. Therefore, the selective adsorption of peripheral proteins to membranes and the binding of lipids to transmembrane proteins are likely to be regulated by specific protein–lipid interactions, not by any inherent conformational restrictions of the lipids. Our results pave the way to comprehensive understanding of lipid–protein interactions in biomedical applications, in particular in lipid-mediated signaling.

INTRODUCTION

Chemical compositions of hydrophilic lipid headgroups vary between different organelles and organisms, and different lipid types regulate protein functions in many different ways [1, 2]. Lipids can directly bind to proteins, or indirectly affect protein functions by altering membrane properties such as charge or elasticity [1, 3]. Specific interactions with certain lipid headgroups are known to be essential for the function of several proteins [3, 4], but it is not clear if the specificity arises from the differences in accessible conformations between lipid types or from specific intermolecular lipid–protein interactions.

Structures of protein-bound lipids are available in the Protein Data Bank (PDB) [5], and crystal structures of lipids have been determined [6, 7], but their relation to the conformational ensembles in bulk membranes in the liquid lamellar

phase remains unclear [8]. The most accurate experimental information on conformational ensembles of lipids in this biologically relevant phase are typically derived from NMR experiments, particularly from the C–H bond order parameters S_{CH} measured using ^{2}H NMR [9–11]. According to these experiments, the glycerol backbone conformations are largely similar irrespective of the headgroup [12], and the headgroup conformations are similar in the phosphatidylcholine (PC), phosphatidylethanolamine (PE), and phosphatidylglycerol (PG) lipids, whereas the phosphatidylserine (PS) headgroup is more rigid [6, 13]. Notably, however, the signs of S_{CH} are not accessible from ^{2}H NMR experiments [14], and universal models to map order parameters to structural ensembles are not available [15, 16]. Therefore, it is not clear if the lipid headgroups in a liquid lamellar bilayer exchange between a few restricted conformations, or can fluctuate freely across a wide conformational range.

Here, we use natural abundance ^{1}H-^{13}C solid-state NMR experiments and MD simulations from the NMRlipids Project to resolve differences in the conformational ensembles of PC, PE, PG, and PS lipid headgroups. Zwitterionic PC are the most common lipids in eukaryotes and PE in bacteria [2, 17]; PE is also the second most abundant glycerophospholipid in eukaryotic cells and has been related to various diseases [18–20]. PS are the most common negatively charged lipids in eukaryotes and PG in bacteria, and both are known to affect membrane protein functionality and signaling [3, 17, 21, 22]. All the four studied lipid types specifically bind to various proteins [23]; we therefore elucidate also the effect of protein binding to headgroup conformations. Similarity of glycerol backbone and headgroup order parameters in model membranes and bacteria [12, 24, 25] suggest that our results can be used to understand the biological role of lipid headgroups in lipid–protein interactions. These interactions are crucial, for example, in lipid-mediated signaling [3] and for the design of phoshopolipid-specific antibodies [26].

METHODS

Experimental C–H bond order parameters

The headgroup and glycerol backbone C–H bond order parameters of 1-palmitoyl-2-oleoyl-sn-glycero-3-phosphoethanolamine (POPE) and 1-palmitoyl-2-oleoyl-sn-glycero-3-phospho-(1'-rac-glycerol) (POPG), purchased from Avanti polar lipids, were measured using natural abundance ^{1}H-^{13}C solid state NMR spectroscopy as described previously [27, 28]. The samples were prepared by simply mixing the lipids with water until a homogeneous preparation of multi-lamellar vesicles (MLVs) was attained and left to equilibrate for approximately 24 hours before measurements. The magnitudes of the order parameters were determined using a R-type Proton Detected Local Field (R-PDLF) experiment [29], and the order parameter signs from S-DROSS experiments [30] combined with SIMPSON simulations [31].

The set-up of the solid-state NMR experiments were identical as in our previous work [32]. The POPE experiments were recorded at 310 K and POPG experiments at 298 K, where the bilayers are in the liquid disordered phase [33].

Glycerol backbone peaks from both lipids, and the α-carbon peak from POPE in the INEPT spectra were assigned based on previously measured POPC spectra [27]. The β-carbon peak from POPE was assigned based on ^{13}C chemical shift table for amines available at https://www.chem.wisc.edu/areas/reich/nmr/c13-data/cdata.htm. The asignment of the α, β, and γ peaks of POPG was based on the measured R-PDLF dipolar couplings in comparison to the known order parameters from previous ^{2}H NMR experiments [13, 34]. The β-carbon peak from POPG overlapped with the g_2 peak from glycerol backbone because their chemical environments are similar.

Molecular dynamics simulations

Molecular dynamics simulation data were collected and analyzed using the methods from the NMRlipids Open Collaboration project (nmrlipids.blogspot.fi) [14, 32, 35, 36]. Simulation details, accessibility information and quality evaluation of approximately 70 combinations of lipid headgroup and force field simulated for this work are in the supplementary information.

Best models for the interpretation of lipid headgroup conformational ensembles from the experimental data were selected using quality evaluation measures defined in the NMRlipids project. Conformational ensembles of headgroup and glycerol backbone in PE and PG simulations were evaluated using the C–H bond order parameters [35]. Interactions between different headgroups were evaluated by monitoring the changes in headgroup order parameters upon mixing the lipids [32]. The ion binding affinities and response of lipids to bound charge were evaluated by monitoring the changes in lipid headgroup order parameters [32, 36].

The differences in headgroup conformation ensembles were analyzed calculating the distributions of six dihedral angles, O_α-C_α-C_β-N/C_γ, P-O_α-C_α-C_β, O_{g3}-P-O_α-C_α, g_3-O_{g3}-P-O_α, g_2-g_3-O_{g3}-P, and g_1-g_2-g_3-O_{g3}, labeled in Fig. 1 C. Relative energy costs for turning dihedral angles with respect to the most probable value (lowest energy) were estimated from the inverse Boltzmann formula $\Delta E(\theta) = -kT\left[\ln[p(\theta)] - \ln[p(\theta_0)]\right]$, where $p(\theta)$ is the dihedral angle distribution and θ_0 is the most probable angle from MD simulation.

Analysis of protein-bound lipid conformations

Lipid structures from the Protein Data Bank (PDB, [38]) were searched using PDBe REST API (www.ebi.ac.uk/pdbe/pdbe-rest-api) using the ligand names listed in
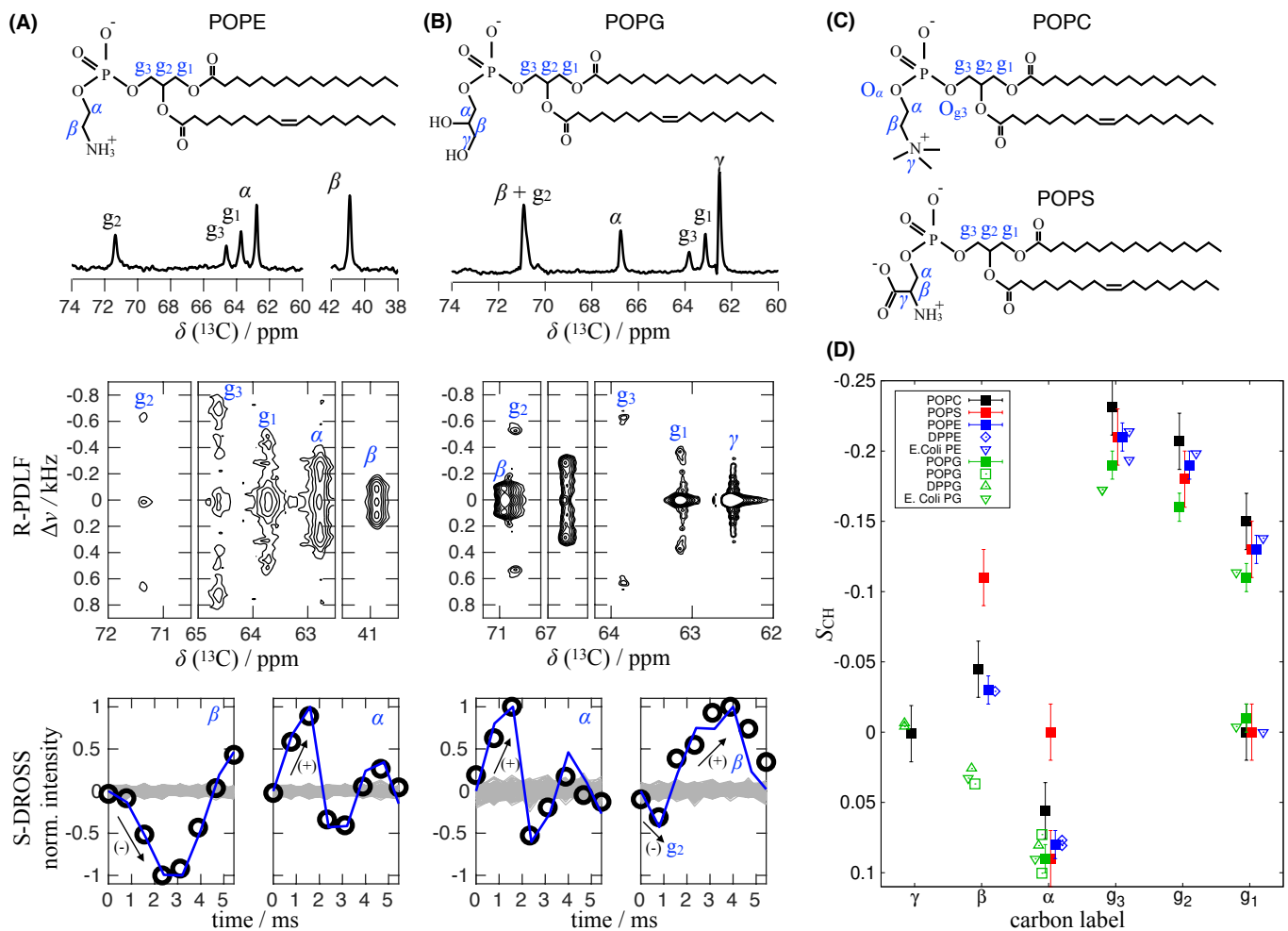
FIG. 1: Chemical structure, refocused-INEPT spectrum, 2D R-PDLF spectra, and S-DROSS dipolar slices (from top to bottom) for **A)** POPE and **B)** POPG MLVs measured by ^{1}H-^{13}C solid-state NMR. The S-DROSS dipolar slices show both experimental data (open circles) and the result of NMR numerical simulations (blue solid lines). Full NMR spectra are shown in Figs. S1 and S2. **C)** Chemical structure of POPC and POPS. **D)** Headgroup and glycerol backbone C-H bond order parameters for different phospholipids measured in the lamellar liquid disordered phase. Filled squares show S_{CH} magnitudes and signs determined by ^{1}H-^{13}C NMR spectroscopy for POPE (310 K) and POPG (298 K), as measured in this work, and from data previously reported for POPS (298 K) [32] and POPC (300 K) [27, 28]. Empty symbols show headgroup and glycerol backbone S_{CH} magnitudes measured previously with ^{2}H NMR and are also plotted as real values using the signs determined in this work for POPG with 10nM PIPES (298 K) [34], DPPG with 10mM PIPES and 100mM NaCl (314 K) [13], DPPE (341 K) [37], E. coli PE and E. coli PG (310 K) [12] .

the supplementary information. Dihedral distributions from the lipid structures were calculated using the MDAnalysis Python library [39, 40] and Jupyter notebook available from *scripts/PDBanalysis.ipynb* folder in Ref 41. Only the structures determined using X-ray crystallography or Cryo-EM with a resolution higher than 3.2 Å were used in the analysis. Some structures of multimeric proteins contained multiple lipids in the same conformation. The conformations were considered identical if all dihedral angles were the same within 3 degrees. In these cases, this conformation was counted only once for the subsequent analyses to avoid its overweighting.

To demonstrate the existence of similar structures of different lipids bound to different proteins, we searched for pairs having the last five heavy atom dihedrals angles in the head-group end (excluding g_1-g_2-g_3-O_{g3} from the list in previous section) within 30 degrees of each other among the structures with resolution higher than 2.5 Å. The two most representative examples were handpicked from the results.

RESULTS AND DISCUSSION

Differences between lipid headgroups from ^{13}C NMR experiments

To experimentally characterize the differences in head-group conformational ensembles of lipids that are not bound to proteins, we measured the C–H bond order parameters and
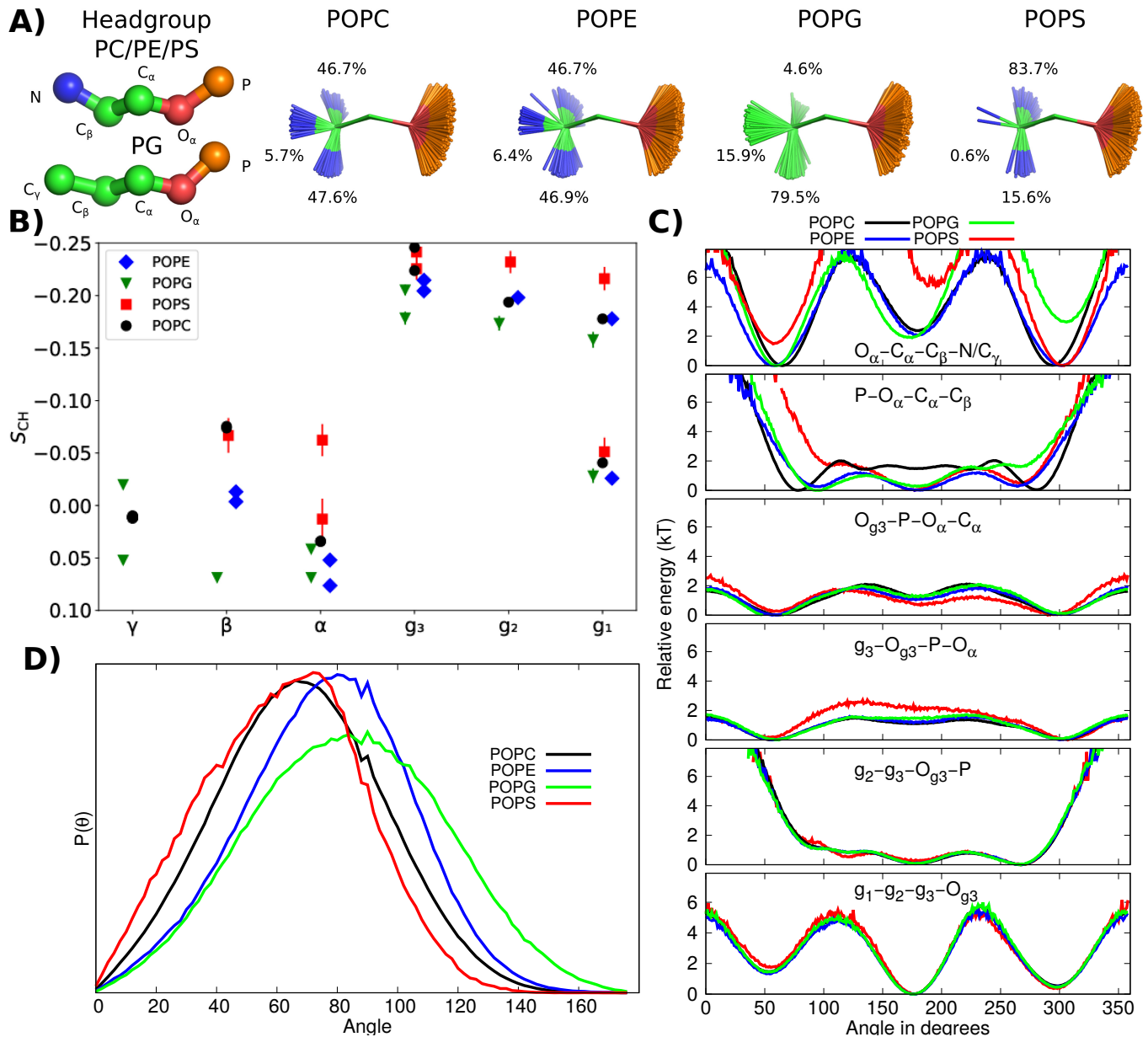
FIG. 2: Results from the best simulation model demonstrating the differences in conformational ensembles between different lipids. The best simulation model (CHARMM36) was selected from the comparison of ten different force fields based on quality evaluation against experimental S_{CH} values in Figs. S3 and S4. **A)** Snapshots with overlayed C_β, C_α and O_α atoms and occurrence of different conformations. **B)** Headgroup and glycerol backbone region order parameters of different lipids. **C)** Relative energies for individual heavy atom dihedral angles estimated from the inverse Boltzmann formula. Angles corresponding to energies above 7 k_BT are not shown because they are not observed in simulations. **D)** Distributions of P–N/C_γ vector angle with respect to membrane normal.

their signs of POPG and POPE in the liquid lamellar phase, as we did previously for POPC and POPS [27, 28, 32]. Determination of headgroup and glycerol backbone order parameters and their signs was straightforward from the data in Figs. 1, S1 and S2 for all the C–H bonds, except for the β and g_2 carbons in POPG. These carbons have overlapping peaks in the INEPT spectra due to their similar chemical environments, and only the magnitude of the larger order parameter could be determined from the R-PDLF spectra (Fig. 1B). Based on previous

^{2}H NMR measurements [12, 13, 34], we assigned the larger order parameter to the g_2 carbon and used the literature value for the β-carbon in SIMPSON simulations to determine the signs. The decrease in the beginning of the S-DROSS curve suggests that the sign of larger g_2 order parameter is negative and later increase suggests that sign of smaller β order parameter is positive as confirmed by the SIMPSON simulations (Fig. 1B).

Experimental order parameters of POPC, POPE, POPG and

POPS glycerol backbones and headgroups from this and previous studies are displayed in Fig. 1D, where the signs from ^{13}C NMR experiments are used also for the ^{2}H NMR data from the literature. The overall agreement of order parameters determined by different research teams and different techniques for the same lipid headgroup is excellent (within ± 0.02 here and in previous studies [14, 32, 35]. Therefore, the differences between lipid types are dictated by the headgroup chemistry rather than inaccuracies in experiments, differences in the acyl chains, or in experimental conditions.

The most distinct order parameters are observed for PS headgroups, for which the α-carbon order parameter exhibits significant forking (different values for different hydrogens bound to the same carbon) and the β-carbon has a more negative value than other studied lipid types. On the other hand, the β-carbon order parameter of PG headgroup has a positive sign, in contrast to all the other lipid types. The sign has not been previously known from ^{2}H NMR experiments which enable detecting only order parameter absolute values [12, 13, 34]. The glycerol backbone order parameters are similar for all the lipid types, although they move slightly toward positive values (closer to zero) in the order PC < PE < PS < PG. Only minor differences between PC and PE headgroups are observed.

Conformational ensembles of different lipid headgroups from MD simulations

MD simulations could be used to interpret the lipid conformational ensembles from experiments due to their direct connection to the measured C-H bond order parameters S_{CH}. To find the best MD simulation models (force fields) for this purpose, we took advantage of the power of the NMRlipids Project, an open science collaboration that has gathered a massive number of simulation trajectories, allowing the evaluation of all the available force fields of PC [35], PS [32], PE (Fig. S3), and PG (Fig. S4) lipids against NMR data. The comparison of hundreds of simulation trajectories simulated with approximately 20 different force fields revealed that none of them can correctly capture the lipid conformational ensembles and reproduce the experimental S_{CH} of all segments within experimental error. However, CHARMM36, the force field showing the best agreement with experiments, correctly captures the essential differences between the PC, PE, PG, and PS headgroup order parameters (compare Figs. 1D and 2 B).

To understand the structural origin of distinct order parameters for the distinct lipids, we first calculated the heavy atom dihedral angle distributions from the best performing simulations that reproduced the differences between headgroups (Fig. S11). Then, we used the inverse Boltzmann formula to estimate the energy costs for different dihedral angle orientations. The results in Fig. 2C suggest that all lipid headgroups are very flexible and energy costs for rotating individual dihedrals to almost any angle is low (below 7 $k_{\mathrm{B}}T$). Only *cis* states of P-O$_\alpha$-C$_\alpha$-C$_\beta$ and g$_2$-g$_3$-O$_{g_3}$-P have larger

relative energies and are not observed for any lipids during the simulations.

Major differences between headgroups are observed for the last two dihedrals in the headgroup end, O$_\alpha$-C$_\alpha$-C$_\beta$-N/C$_\gamma$ and P-O$_\alpha$-C$_\alpha$-C$_\beta$, which prefer *gauche$^-$* conformations for PG and *gauche$^+$* for PS, whereas PC and PE exhibit symmetric distributions. Also, the energy barriers for O$_\alpha$-C$_\alpha$-C$_\beta$-N/C$_\gamma$ dihedral rotations between *gauche* and *trans* states are larger for PS and PG lipids than for PC and PE lipids. The rest of the dihedrals are similar between different lipids, with the exception of PS lipids for which slightly larger energy for *eclipsed anti* conformation in g$_3$-O$_{g_3}$-P-O$_\alpha$ dihedral was observed. Therefore we suggest that the main differences between lipid headgroups leading to distinct order parameters occur in the headgroup end, while in the phosphate region they remain similar in different lipids with the exception of PS. The increased barriers for dihedral rotations may explain the more rigid headgroup structures in PS [6, 43]. Furthermore, the angle between headgroup dipole and membrane normal decreases in the order of PG > PE > PC > PS (Fig. 2D). However, the differences between PC and PE in P-O$_\alpha$-C$_\alpha$-C$_\beta$ dihedral and P–N vector dipole may be artificial as the β-carbon order parameter in PC is too negative even in the best available force field, thereby not being equal to the order parameter in PE as observed in experiments [35].

In conclusion, all studied lipid headgroups sample very broad conformational ensembles in the liquid lamellar phase and the sampled dihedral angles are within similar ranges for all headgroup types. Since the rotation of dihedral angles to almost any position bears relatively low energy cost, the lipid headgroups are able to adopt a wide range of conformations when interacting with proteins, ions, or other biomolecules. Therefore, the structures in lipid crystals [6, 7] are not representative of the liquid state, and models aiming to explain NMR data using only a few conformations [9–11, 16] are not sufficient to capture the large conformational space of lipids in the liquid lamellar state. However, conformational ensembles of lipids in MD simulation trajectories with accurate force fields that capture the experimental NMR order parameters and can be considered realistic, and thereby used to interpret the experimental data.

Lipid conformational ensembles in charged membranes

Charged entities, such as lipids, proteins, surfactants, drugs, and ions incorporated in membranes can change the orientation of the headgroup dipole in PC lipids and affect the order parameters of the lipid headgroups [44]. However, the detailed understanding of the structural and energetic responses of lipids to membrane-bound electric charge is still lacking [11].

To resolve lipid headgroup conformational ensembles in cellular membranes bearing positive charge, we calculated the heavy atom dihedral angle distributions from the subset of simulations that correctly captured the experimentally mea-
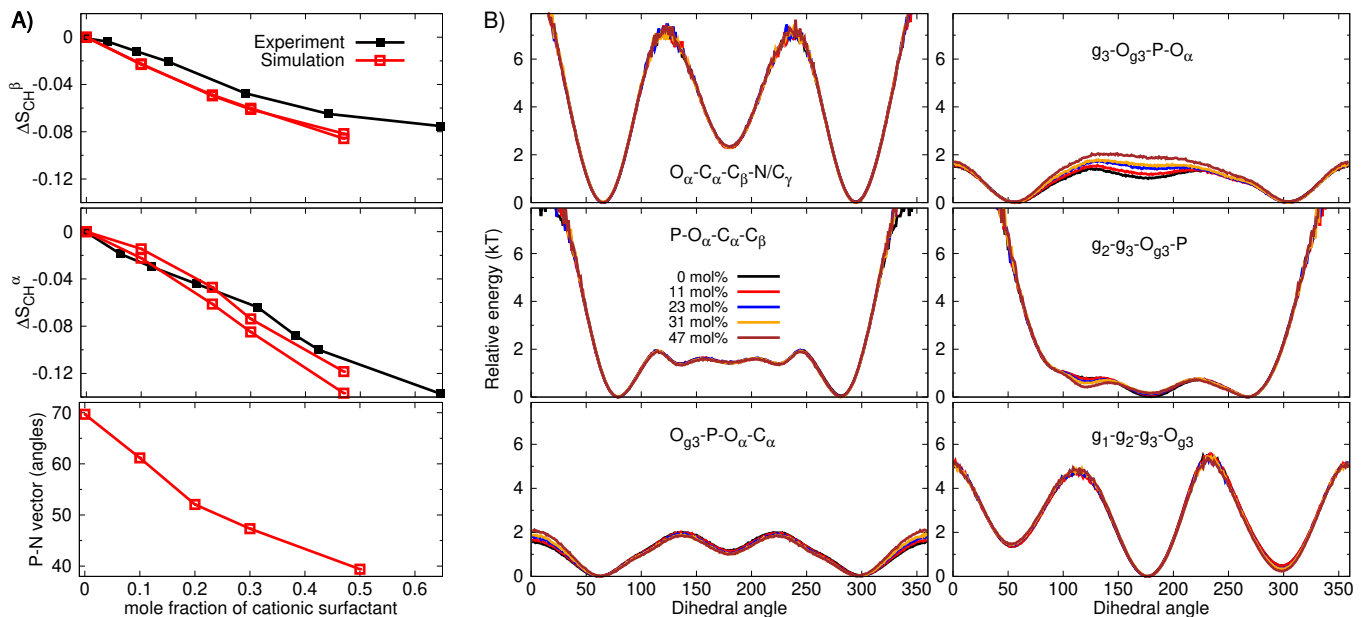
FIG. 3: **A)** Modulation of PC headgroup order parameters and P–N vector tilt (angle between the P-N vector and the bilayer normal) upon addition of cationic surfactant (dihexadecyldimethylammonium) from CHARMM36 simulations compared with the experimental data [42]. **B)** Relative energies for individual dihedral angles estimated from inverse Boltzmann distributions of heavy atom dihedral angles with different amounts of cationic surfactant from CHARMM36 simulations.

sured decrease in PC headgroup order parameters upon addition of cationic surfactants into a bilayer (figure 3 A). The dihedral angle distributions and relative energies in figures S12 and 3 B reveal that the addition of positive charge into a membrane decreases the abundance of *trans* states in g_2-g_3-O_{g_3}-P and g_3-O_{g_3}-P-O_α, and *cis* states in O_{g_3}-P-O_α-$C\alpha$ dihedrals. The choline region remains essentially unchanged and only minor changes are observed in the other dihedrals even at a surfactant molar fraction of 0.47.

In addition, binding of ions to the membrane may affect the lipid headgroup conformational ensembles under physiological conditions. The bound Ca^{2+} ion to PC headgroup leads to similar decrease in trans state probability for g_3-O_{g3}-P-O_α dihedral in the most realistic MD simulation models as observed for cationic surfactants (lipid17ecc and CHARMM36 in Figs. S13, S14 and Fig. S7). The dihedral distributions of the PG headgroup are more sensitive to the bound ions in the most realistic simulations, but upward tilting of the headgroup dipole upon the addition of $CaCl_2$ is weaker than in PC (Lipid17 and Slipids in Figs. S7, S15 and S16). However, the changes in PG lipid dihedrals upon the addition of $CaCl_2$ differ between the best models (Figs. S15 and S16), and none of the simulations captures the Ca^{2+} ion binding affinity and conformational ensemble of PG lipids simultaneously. Moreover, experimental data to evaluate the response of α-carbon order parameters to the added $CaCl_2$ in PG is not available. Additionally, the headgroup conformational ensembles in mixtures of PC and charged (PG or PS) or zwitterionic (PE) lipids could not be resolved with the currently available force fields and experimental data (Figs. S5 and S6,

and Ref. [32, 45, 46]).

In conclusion, the MD simulation results suggest that the structural response of lipid headgroups to membrane-bound charges arises from mild changes in dihedral angle distributions, rather than restriction of lipids to fixed conformations. Therefore, lipid headgroups sample a large space of different conformations also in charged membranes, thereby retaining the capability to adopt multiple conformations when interacting with proteins or other molecules.

Protein-bound lipid conformations

Interpretation of experimental order parameters using MD simulations in previous sections suggest that PC, PE, PG, and PS lipid headgroups are very flexible, allowing them to bind proteins in various different conformations. To test this prediction, we analyzed the conformations of all protein-bound lipids from structures deposited in the PDB [5]. We found 311 PC, 394 PE, 154 PG, and 35 PS lipid conformations that were bound to different types of proteins (including both integral and peripheral membrane proteins) and were determined as a part of protein structure using crystallography or cryo-EM. The full list of structures with bound lipids is available from *Data/PDBdistributions/pdbtable.pdf* in Ref. [41].

The heavy atom dihedral angle distributions calculated from these conformations (Fig. 4 A) reveal that the protein-bound lipids indeed exhibit a wide range of conformations, independent of the headgroup type. As for bulk lipid bilayers (Figs. 2C, S11), only *cis* conformations of P-O_α-C_α-C_β
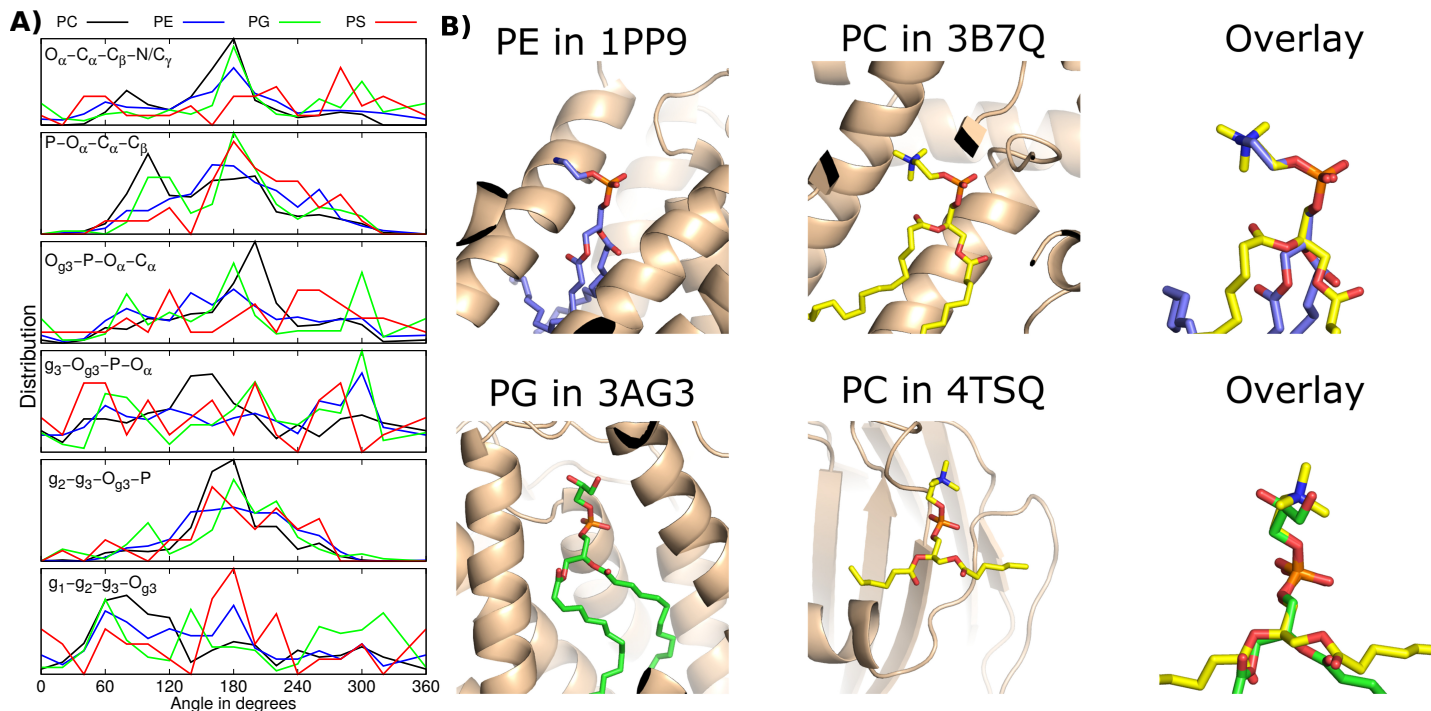
FIG. 4: A) Heavy atom dihedral angle distributions calculated from lipid structures in PDB. B) The structure of PE headgroup bound to cytochrome bc_1 complex (PDB ID: 1PP9 [47]) with identical conformation as the PC headgroup bound to yeast Sec14 (PDB ID: 3B7Q [48]), and the structure of PG headgroup bound to bovine cytochrome c oxidase (PDB ID: 3AG3 [49]) with identical conformation as PC to FraC, a pore-forming toxin (PDB ID: 4TSQ [50]).

and g_2-g_3-O_{g_3}-P dihedrals are almost completely absent in all lipids, and significant differences between different headgroups are not observed. Structures deviating from lipid crystals have been previously proposed to indicate inaccuracies in lipid structures in PDB [8, 15]. However, we observe large deviations from the lipid crystal structures also in conformational ensembles that reproduce the NMR data in the liquid lamellar phase, indicating that such deviations are realistic also in the protein-bound states.

Our results suggest that flexible lipid headgroups can optimize the intermolecular interactions with proteins by binding in a wide range of conformations. Therefore, the specific binding of lipids to proteins is not driven by differing structural preferences between headgroups. This is demonstrated in Fig. 4 B with two examples where different lipid types bound to different proteins have almost identical headgroup conformations: PE in cytochrome bc_1 complex is similar to PC bound to yeast Sec14, and PG bound to bovine cytochrome c oxidase is similar to PC bound to pore-forming toxin (FraC). On the other hand, a single lipid headgroup type is capable of accommodating various binding positions and as such would be able to specifically bind to many different kinds of binding sites.

CONCLUSIONS

C–H bond order parameters S_{CH} from NMR experiments suggest that lipid headgroup conformational ensembles depend on lipid type (PC, PE, PG, or PS) and membrane charge (cationic lipids, surfactants, accumulated ions or drugs). Our analysis of these data, using MD simulations collected within the NMRlipids Project, revealed that the differences in S_{CH} can be explained by small changes in the dihedral angle probability distributions. All four studied headgroup types (PC, PE, PG, and PS) are flexible and access a similarly wide range of conformations, with very few restrictions in dihedral orientations—also when membranes are charged. In conclusion, the observed differences in S_{CH} originate from slightly reweighed conformational probabilities rather than changes in accessible structures.

The flexibility and wide conformational space of headgroups suggest that protein–bound lipids can adapt to various binding sites to optimize the lipid–protein interactions. We tested this prediction by analyzing from PDB the conformations of lipids that are tightly bound to proteins. We found that also the protein-bound lipids exhibit a wide range of conformations, without significant differences between different lipid types: The specificity of lipid binding to proteins is not regulated by accessible lipid structures, but a single lipid type can adapt to various binding pockets.

Our results pave the way toward understanding lipid-

mediated cell signaling and how lipids regulate membrane protein function in general. We suggest that the key to understanding selective binding of certain lipid types to proteins is in intermolecular lipid–protein interactions, rather than in conformational restrictions inherent to the lipids. The broad conformational ensembles we see in bulk bilayers suggest that the structures observed in pure lipid crystals occur seldomly in liquid state. Consequently, in protein binding the entropic cost on the lipid may be significant.

* samuli.ollila@helsinki.fi

[1] A. Lee, Biochimica et Biophysica Acta (BBA) - Biomembranes **1612**, 1 (2003), ISSN 0005-2736, URL http://www.sciencedirect.com/science/article/pii/S0005273603000567.

[2] G. van Meer, D. R. Voelker, and G. W. Feigenson, Nature Reviews Molecular Cell Biology **9**, 112 (2008), URL https://doi.org/10.1038/nrm2330.

[3] M. A. Lemmon, Nat. Rev. Mol. Cell Biol. **9**, 99 (2008).

[4] A. G. Lee, Trends in Biochemical Sciences **36**, 493 (2011), URL https://doi.org/10.1016/j.tibs.2011.06.007.

[5] H. M. Berman, J. Westbrook, Z. Feng, G. Gilliland, T. N. Bhat, H. Weissig, I. N. Shindyalov, and P. E. Bourne, Nucleic Acids Research **28**, 235 (2000), ISSN 0305-1048, https://academic.oup.com/nar/article-pdf/28/1/235/9895144/280235.pdf, URL https://doi.org/10.1093/nar/28.1.235.

[6] G. Büldt and R. Wohlgemuth, The Journal of Membrane Biology **58**, 81 (1981), ISSN 1432-1424, URL http://dx.doi.org/10.1007/BF01870972.

[7] I. Pascher, M. Lundmark, P.-G. Nyholm, and S. Sundell, Biochim. Biophys. Acta **1113**, 339 (1992).

[8] D. Marsh and T. Páli, European Biophysics Journal **42**, 119 (2013), URL https://doi.org/10.1007/s00249-012-0816-6.

[9] J. Seelig, Q. Rev. Biophys. **10**, 353 (1977).

[10] J. H. Davis, Biochim. Biophys. Acta **737**, 117 (1983).

[11] D. J. Semchyschyn and P. M. Macdonald, Magn. Res. Chem. **42**, 89 (2004).

[12] H. U. Gally, G. Pluschke, P. Overath, and J. Seelig, Biochemistry **20**, 1826 (1981).

[13] R. Wohlgemuth, N. Waespe-Sarcevic, and J. Seelig, Biochemistry **19**, 3315 (1980).

[14] O. S. Ollila and G. Pabst, Biochim. Biophys. Acta **1858**, 2512 (2016).

[15] W. Pezeshkian, H. Khandelia, and D. Marsh, Biophysical Journal **114**, 1895 (2018), ISSN 0006-3495, URL http://www.sciencedirect.com/science/article/pii/S0006349518302467.

[16] H. Akutsu, Biochimica et Biophysica Acta (BBA) - Biomembranes **1862**, 183352 (2020), URL https://doi.org/10.1016/j.bbamem.2020.183352.

[17] C. Sohlenkamp and O. Geiger, FEMS Microbiology Reviews **40**, 133 (2015).

[18] J. E. Vance, Traffic **16**, 1 (2015).

[19] E. Calzada, O. Onguka, and S. M. Claypool (Academic Press, 2016), vol. 321 of *International Review of Cell and Molecular Biology*, pp. 29 – 88.

[20] D. Patel and S. N. Witt, Oxidative Medicine and Cellular Longevity **2017**, 4829180 (2017).

[21] P. A. Leventis and S. Grinstein, Annual Review of Biophysics **39**, 407 (2010).

[22] P. Hariharan, E. Tikhonova, J. Medeiros-Silva, A. Jeucken, M. V. Bogdanov, W. Dowhan, J. F. Brouwers, M. Weingarth, and L. Guan, BMC Biology **16**, 85 (2018).

[23] P. L. Yeagle, Biochimica et Biophysica Acta (BBA) - Biomembranes **1838**, 1548 (2014), membrane Structure and Function: Relevance in the Cell's Physiology, Pathology and Therapy.

[24] P. Scherer and J. Seelig, EMBO J. **6** (1987).

[25] J. Seelig, Cell Biology International Reports **14**, 353 (1990), ISSN 0309-1651, URL http://www.sciencedirect.com/science/article/pii/030916519091204H.

[26] F. Vigant, N. C. Santos, and B. Lee, Nature Reviews Microbiology **13**, 426 (2015).

[27] T. M. Ferreira, F. Coreta-Gomes, O. H. S. Ollila, M. J. Moreno, W. L. C. Vaz, and D. Topgaard, Phys. Chem. Chem. Phys. **15**, 1976 (2013).

[28] T. M. Ferreira, R. Sood, R. Bärenwald, G. Carlström, D. Topgaard, K. Saalwächter, P. K. J. Kinnunen, and O. H. S. Ollila, Langmuir **32**, 6524 (2016).

[29] S. V. Dvinskikh, H. Zimmermann, A. Maliniak, and D. Sandstrom, J. Magn. Reson. **168**, 194 (2004).

[30] J. D. Gross, D. E. Warschawski, and R. G. Griffin, J. Am. Chem. Soc. **119**, 796 (1997).

[31] M. Bak, J. T. Rasmussen, and N. C. Nielsen, Journal of Magnetic Resonance **147**, 296 (2000), ISSN 1090-7807, URL http://www.sciencedirect.com/science/article/pii/S1090780700921797.

[32] H. Antila, P. Buslaev, F. Favela-Rosales, T. M. Ferreira, I. Gushchin, M. Javanainen, B. Kav, J. J. Madsen, J. Melcr, M. S. Miettinen, et al., J. Phys. Chem. B **123**, 9066 (2019).

[33] D. Marsh, *Handbook of Lipid Bilayers, Second Edition* (RSC press, 2013).

[34] F. Borle and J. Seelig, Chem. Phys. Lipids **36**, 263 (1985).

[35] A. Botan, F. Favela-Rosales, P. F. J. Fuchs, M. Javanainen, M. Kanduč, W. Kulig, A. Lamberg, C. Loison, A. Lyubartsev, M. S. Miettinen, et al., J. Phys. Chem. B **119**, 15075 (2015).

[36] A. Catte, M. Girych, M. Javanainen, C. Loison, J. Melcr, M. S. Miettinen, L. Monticelli, J. Maatta, V. S. Oganesyan, O. H. S. Ollila, et al., Phys. Chem. Chem. Phys. **18**, 32560 (2016).

[37] J. Seelig and H. U. Gally, Biochemistry **15**, 5199 (1976).

[38] H. M. Berman, J. Westbrook, Z. Feng, G. Gilliland, T. N. Bhat, H. Weissig, I. N. Shindyalov, and P. E. Bourne, Nucleic Acids Research **28**, 235 (2000), ISSN 0305-1048.

[39] N. Michaud-Agrawal, E. J. Denning, T. B. Woolf, and O. Beckstein, J. Comput. Chem. **32**, 2319 (2011), https://onlinelibrary.wiley.com/doi/pdf/10.1002/jcc.21787, URL https://onlinelibrary.wiley.com/doi/abs/10.1002/jcc.21787.

[40] Richard J. Gowers, Max Linke, Jonathan Barnoud, Tyler J. E. Reddy, Manuel N. Melo, Sean L. Seyler, Jan Domaski, David L. Dotson, Sbastien Buchoux, Ian M. Kenney, et al., in *Proceedings of the 15th Python in Science Conference*, edited by Sebastian Benthall and Scott Rostrup (2016), pp. 98 – 105.

[41] N. project, *Nmrlipidsivb github repository*, URL https://github.com/NMRLipids/NMRlipidsIVPEandPG.

[42] P. G. Scherer and J. Seelig, Biochemistry **28**, 7720 (1989).

[43] J. L. Browning and J. Seelig, Biochemistry **19**, 1262 (1980).

[44] J. Seelig, P. M. MacDonald, and P. G. Scherer, Biochemistry **26**, 7535 (1987).

[45] A. Melcrová, S. Pokorna, S. Pullanchery, M. Kohagen, P. Jurkiewicz, M. Hof, P. Jungwirth, P. S. Cremer, and L. Cwiklik, Sci. Reports **6**, 38035 (2016).

[46] J. Melcr, T. M. Ferreira, P. Jungwirth, and O. H. S. Ollila, J. Chem. Theo. Comput. **16**, 738 (2020).

[47] L. shar Huang, D. Cobessi, E. Y. Tung, and E. A. Berry, Journal of Molecular Biology **351**, 573 (2005), ISSN 0022-2836, URL https://www.sciencedirect.com/science/article/pii/S0022283605006078.

[48] G. Schaaf, E. A. Ortlund, K. R. Tyeryar, C. J. Mousley, K. E. Ile, T. A. Garrett, J. Ren, M. J. Woolls, C. R. Raetz, M. R. Redinbo, et al., Molecular Cell **29**, 191 (2008), ISSN 1097-2765, URL https://doi.org/10.1016/j.molcel.2007.11.026.

[49] K. Muramoto, K. Ohta, K. Shinzawa-Itoh, K. Kanda, M. Taniguchi, H. Nabekura, E. Yamashita, T. Tsukihara, and S. Yoshikawa, Proceedings of the National Academy of Sciences **107**, 7740 (2010), ISSN 0027-8424, https://www.pnas.org/content/107/17/7740.full.pdf, URL https://www.pnas.org/content/107/17/7740.

[50] K. Tanaka, J. M. Caaveiro, K. Morante, J. M. González-Mañas, and K. Tsumoto, Nature Communications **6**, 6337 (2015), ISSN 2041-1723, URL https://doi.org/10.1038/ncomms7337.